

Mouse Visual Cortex Modelling

The impact of an ecological data diet on the neural predictivity of CNNs

Giacomo Amerio, Giovanni Lucarelli, Andrea Spinelli

github.com/giovanni-lucarelli/mice-representation

1 Introduction

Studies of the mouse visual system have identified a range of cortical areas that support diverse visual behaviors, including stimulus-reward associations, goal-directed navigation, and object-centered discrimination. Despite extensive investigation, a comprehensive understanding of the mouse visual cortex and its functional organization remains incomplete.

Nayebi *et al.* [4] demonstrated that a shallow neural network architecture trained with a self-supervised objective and low-resolution visual inputs provides an optimal model of the mouse visual cortex. Their findings suggest that a lightweight, general-purpose visual system can effectively account for mouse visual representations. Acknowledging the inherently low visual acuity of mice, Nayebi *et al.* achieved improved neural predictivity by training their network on lower-resolution images. They used image resolution as a proxy for mouse visual acuity, rather than employing a biologically informed image preprocessing pipeline to approximate this property. They reported optimal neural predictivity using 64×64 pixel images and proposed that future work should incorporate more realistic, neurophysiologically informed preprocessing approaches.

The goal of this project is to extend Nayebi’s analysis by developing and evaluating such preprocessing pipeline. Specifically, this study aims to investigate whether biologically informed visual transformations improve neural predictivity. Our findings indicate that the proposed ecological data diet yields higher neural predictivity compared to a traditional ImageNet-pretrained model. Moreover, a post-hoc analysis revealed that applying the data diet at inference time has a substantial impact on models trained without it. Together, these findings highlight the importance of stimulus realism and preprocessing in modeling mouse visual systems. They also suggest that even simple manipulations of the input distribution can yield large changes in neural predictivity, highlighting a potential confound in Nayebi’s work, where such effects were not controlled for.

2 Methods

2.1 Data Diet

A fair comparison between mouse visual perception and convolutional neural networks (CNNs) should respect the ecological limits of the mouse visual system, especially its limited spatial resolution. Mice have a low visual acuity; behaviorally measured contrast sensitivity functions (CSFs) show a band-pass profile that peaks at about 0.2 cycles per degree [5]. The CSF quantifies the inverse contrast required to detect sinusoidal gratings at each spatial frequency, summarizing the behavior of the early visual pathway.

Following Muratore *et al.* [3], we treat the behavioral CSF as a functional approximation of the animal’s visual system. We search for the combination of Gaussian blur and Gaussian noise that reproduces the mouse CSF measured behaviorally by Prusky. To calibrate these parameters, we simulate the standard grating detection task used in CSF experiments: blurred/noisy sinusoidal gratings are shown against noisy mid-gray images across a range of spatial frequencies and contrasts. The simulated display is divided into patches of 24 pixels; within each patch we compute the contrast as the standard deviation of pixel intensities, and concatenate these patch contrasts into a feature vector. We train a linear SVM to tell apart sinusoidal grating patches from a uniform mid-gray patch, using $n = 5000$ training examples for each class. For the grating class, we randomize orientation and phase. After training, we probe the SVM with gratings at different contrasts and spatial frequencies, and measure how often it correctly reports “grating” instead of “gray.” For each spatial frequency, this accuracy-vs-contrast curve is treated as a psychometric function, from which we read off the contrast level that reaches threshold performance. We then collect those contrast thresholds across spatial frequencies (see fig. 1). To compare the resulting CSF to the mouse CSF, we perform a grid search over blur and noise variance to minimize the (absolute) error between the log contrast thresholds of our model and those measured in mice (see fig. 2). The optimal parameter combination identified by this simulated grating detection task is $blur = 0.176$ and $noise = 0.250$ (see fig. 3).

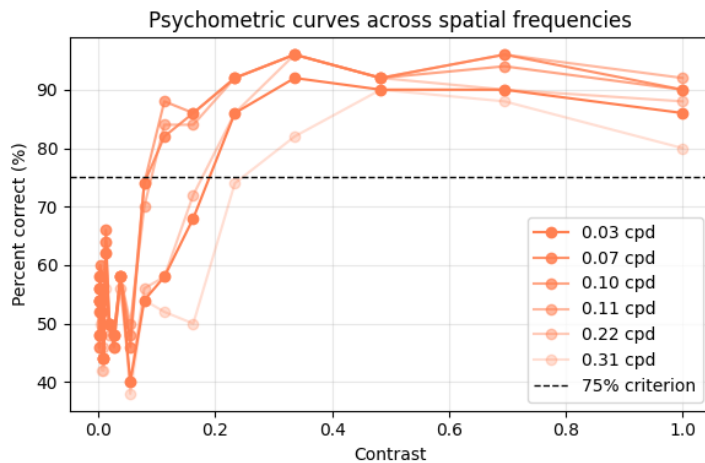


Figure 1: Psychometric curves are shown for different spatial frequencies. The intersection between the fitted psychometric curve and the 75% accuracy criterion is the threshold contrast chosen for the CSF.

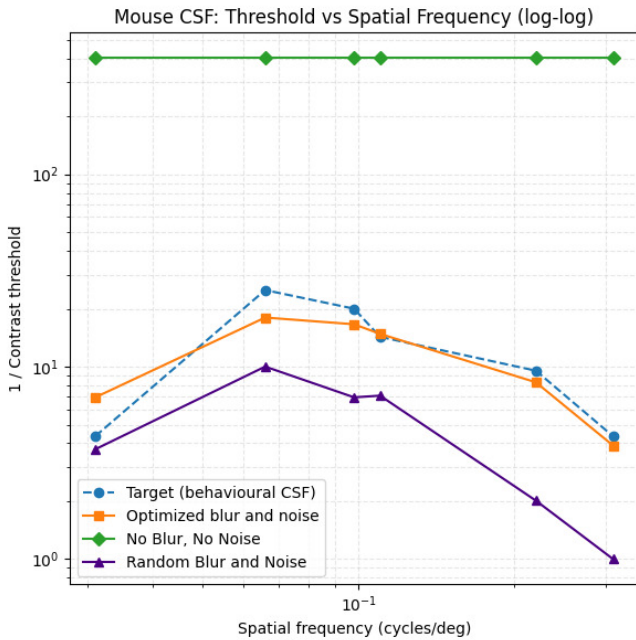


Figure 2: The contrast sensitivity function (CSF) measured for mice by Prusky *et al.* [5] (blue line) is shown along the CSFs obtained for a simulated observer, measuring the contrast of input images in small patches with different blur and noise parameters.

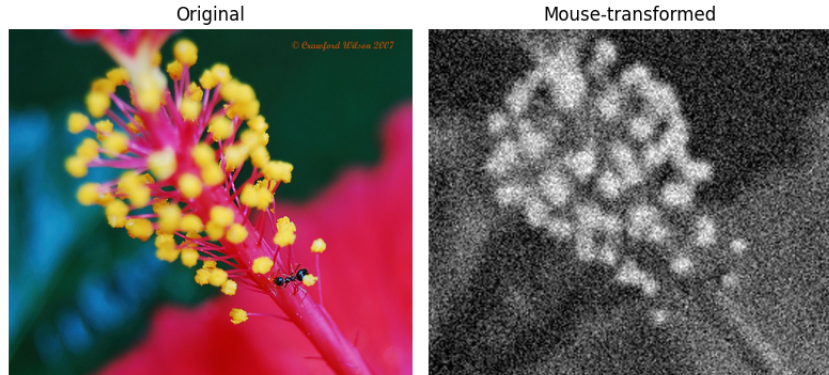


Figure 3: Illustration of an ImageNet sample after applying the optimized “artificial retina” preprocessing. The image has been transformed with a Gaussian blur ($\sigma = 0.176$) and additive Gaussian noise ($\sigma = 0.250$) to match the mouse contrast sensitivity function, as determined by the simulated psychophysical task (see fig. 2).

2.2 Representation Preprocessing

Allen Brain Neuropixels Visual Coding Neuropixels recordings from the Allen Brain Observatory Visual Coding dataset [1] were preprocessed following the methodology described by Nayebi *et al.* [4]. For each specimen and each visual area, we first computed the average temporal response across 10-ms time bins within the 0–250 ms post-stimulus window. This averaging was restricted to the largest contiguous time interval during which the median split-half reliability (computed across the population of recorded units within the specimen) exceeded a threshold of 0.3. Subsequently, for each visual area, we retained only those specimens with a number of responsive units greater than or equal to the 75th percentile across all specimens in that area. After this filtering procedure, the resulting neural response for each stimulus is represented as a real-valued vector, where each element corresponds to the mean response of an individual unit (neuron) to that specific stimulus. These vectors serve as the neural representations used in the subsequent neural mapping analyses.

AlexNet Activations We analyzed multiple variants of the AlexNet architecture, including: (1) an untrained network with Xavier initialization, (2) a pretrained model trained on the ImageNet dataset (PyTorch default), and (3) a pretrained model trained on ImageNet images preprocessed according to our ecological diet. In doing so, AlexNet is constrained to operate over the same spatial bandwidth as the mouse.

For each network, we computed activations in response to the same set of visual stimuli presented to the mice in the Allen Brain dataset. From each convolutional layer, activations were spatially averaged using global average pooling, resulting in a layer-specific feature vector whose dimensionality corresponds to the number of channels in that layer. These vectors constitute the model representations used for subsequent neural correspondence analyses.

	conv1	conv2	conv3	conv4	conv5
Channels	64	192	384	256	256

Table 1: Architecture of the convolutional layers in AlexNet. The number of channels in each layer corresponds to the dimensionality of the representation vector after global average pooling.

2.3 Neural mapping

The metric used in this work to map neuropixel responses to AlexNet activations is the Representation Similarity Analysis (RSA) [2].

Given two neural system X, Y , a set of n stimuli and let $\mathbf{z}_i^{(X)} \in \mathbb{R}^{|X|}, \mathbf{z}_i^{(Y)} \in \mathbb{R}^{|Y|}$ (where in general $|X| \neq |Y|$), be the responses of the two systems to each stimulus i .

We define RSA score

$$\text{RSA}^{(X,Y)} = \text{Corr}(\text{RDM}^{(X)}, \text{RDM}^{(Y)})$$

where

$$\text{RDM}_{i,j}^{(X)} = 1 - \text{Corr}(\mathbf{z}_i^{(X)}, \mathbf{z}_j^{(X)}) , \quad \text{RDM}_{i,j}^{(Y)} = 1 - \text{Corr}(\mathbf{z}_i^{(Y)}, \mathbf{z}_j^{(Y)})$$

and RDM is the Representation Dissimilarity Matrix.

2.3.1 Interanimal consistency

One upper bound of the neural predictivity is defined by the inter-animal predictivity, *i.e.* the RSA score between the mice or equivalently the similarity score of one mouse and all the others. In our analysis a biological neural system is defined by the tuple (s, a) where s is the specimen and a is a visual area.

Corrected RSA The neuropixel data from the Allen Brain dataset are very noisy, hence to produce a robust estimate of the similarity score we used the corrected RSA proposed in Nayebi *et al.* [4], exploiting the presence of different trials for each stimulus.

Let $\mathbf{z}_{i,t}^{(X)} \in \mathbb{R}^{|X|}$ be the representation relative to the neural system $X = (s, a)$ for the stimulus i and the trial $t \in \{1, \dots, T\}$ (in the dataset for each stimulus we have $T = 50$). We define the X_1, X_2 two new neural systems such that $\mathbf{z}_i^{(X_1)} \in \mathbb{R}^{|X|}, \mathbf{z}_i^{(X_2)} \in \mathbb{R}^{|X|}$ are obtained by taking two random halves of trials and computing the average response, for each stimulus, over each subset of trials.

$$\text{RSA}_{\text{corrected}}^{(X,Y)} = \frac{\text{RSA}^{(X,Y)}}{\sqrt{\text{reliability}(X) \cdot \text{reliability}(Y)}}$$

and the reliability of a representation is computed as the similarity between two halves of the trials, using split-half correlation (Spearman-Brown corrected):

$$\text{reliability}(X) = \text{SB}(\text{RSA}^{(X_1, X_2)}), \quad \text{SB}(r) = \frac{2r}{1+r}.$$

The split has been performed 100 times by randomly assigning each trial to one of the two halves, and then averaging the similarity score over the splits.

Pooled interanimal consistency To obtain a more robust estimate of inter-animal similarity, we introduced a pooled version of the corrected RSA, where neural responses from multiple specimens of the same visual area are combined into a single, population-level representation. Specifically, let $\mathcal{S}_a = \{s_1, s_2, \dots, s_S\}$ denote the set of specimens for a fixed area a . For each specimen (s, a) we have trial responses $\mathbf{z}_{i,t}^{(s,a)} \in \mathbb{R}^{|(s,a)|}$ for stimulus i and trial t .

For each source specimen $(s, a) \in \mathcal{S}_a \setminus \{s^*\}$, we randomly split the available trials into two disjoint halves and compute the mean response over each half, obtaining $\mathbf{z}_i^{(s_1,a)}$ and $\mathbf{z}_i^{(s_2,a)}$. The pooled representations are then built by concatenating the averaged responses of all source specimens along the neural feature dimension:

$$\mathbf{z}_i^{(\text{pool}_1,a)} = \bigoplus_{s \in \mathcal{S}_a \setminus \{s^*\}} \mathbf{z}_i^{(s_1,a)}, \quad \mathbf{z}_i^{(\text{pool}_2,a)} = \bigoplus_{s \in \mathcal{S}_a \setminus \{s^*\}} \mathbf{z}_i^{(s_2,a)}.$$

This “population pooling” procedure creates a new aggregate neural system combining information across multiple specimens from the same area.

At each bootstrap iteration, the pooled halves (pool_1, a) and (pool_2, a) are compared with two independent halves (s_1^*, a) and (s_2^*, a) of a held-out target specimen (s^*, a) using the corrected RSA metric defined above. To ensure symmetry, we compute the cross-half similarity:

$$\text{RSA}_{\text{num}} = \frac{1}{2} \left(\text{RSA}^{(\text{pool}_1, a, s_2^*, a)} + \text{RSA}^{(\text{pool}_2, a, s_1^*, a)} \right),$$

and normalize it by the geometric mean of the reliabilities of both the pooled and target systems:

$$\text{RSA}_{\text{pooled}}^{(\text{corr})}(a) = \frac{\text{RSA}_{\text{num}}}{\sqrt{\text{reliability}(\text{pool}, a) \cdot \text{reliability}(s^*, a)}}.$$

The procedure is repeated over 100 random trial partitions, and the final pooled inter-animal consistency score for area a is obtained as the mean and standard deviation of the resulting corrected RSA values.

2.3.2 Neural predictivity

The similarity between AlexNet activations and the neuropixel responses has been computed analogously to what introduced above. Specifically, for each layer l of the convolutional network and (s, a) specimen-area pair, we can define

$$\text{RSA}^{(s, a, l)} = \text{Corr}(\text{RDM}^{(s, a)}, \text{RDM}^{(\text{AlexNet}, l)})$$

and

$$\text{RSA}_{\text{corrected}}^{(s, a, l)} = \frac{\text{RSA}^{(s, a, l)}}{\sqrt{\text{reliability}(s, a)}}$$

where $\text{reliability}(\text{AlexNet}, l) = 1$ for all layers l , since the activations in a forward pass are deterministic.

3 Results

Table 2 reports the number of selected specimens and units after the Allen dataset preprocessing, and the pooled inter-animal consistency (RSA score) computed for each visual area. The mean RSA values, together with their corresponding standard errors of the mean (SEM), quantify the reliability of neural responses across animals within each region.

Area	Specimens	Units per Specimen	IC
AL	6	[85, 127, 184, 91, 166, 89]	0.648 ± 0.021
AM	7	[70, 94, 71, 72, 70, 74, 135]	0.570 ± 0.030
LM	6	[51, 53, 74, 56, 77, 58]	0.453 ± 0.031
PM	5	[65, 115, 62, 90, 54]	0.552 ± 0.020
RL	7	[76, 69, 67, 68, 79, 95, 111]	0.542 ± 0.027
V1	8	[110, 102, 91, 85, 88, 93, 94, 85]	0.592 ± 0.038

Table 2: Number of specimen IDs, total units, units per specimen ID, and interanimal consistency score (\pm standard error) for each visual area.

3.1 Data diet impact

In fig. 4 is shown the RSA score for each visual areas and for each convolutional layer of AlexNet. We can see that the RSA score is higher in the case of data diet both at training and inference time. At training time means that all the ImageNet dataset have been preprocessed with our “mouse-like” pipeline, whereas at inference time means that the pipeline has been applied to the same Allen Brain stimuli that the mice saw.

Specifically, from fig. 5 where the untrained model (baseline) have been subtracted, we can see that, the diet affects negatively the first convolutional layer but leads to higher RSA score in the subsequent layers. Moreover we can observe that in some visual areas, namely AL, LM, RL, V1, for the last two layers the trained models provide a worse score with respect to the untrained one.

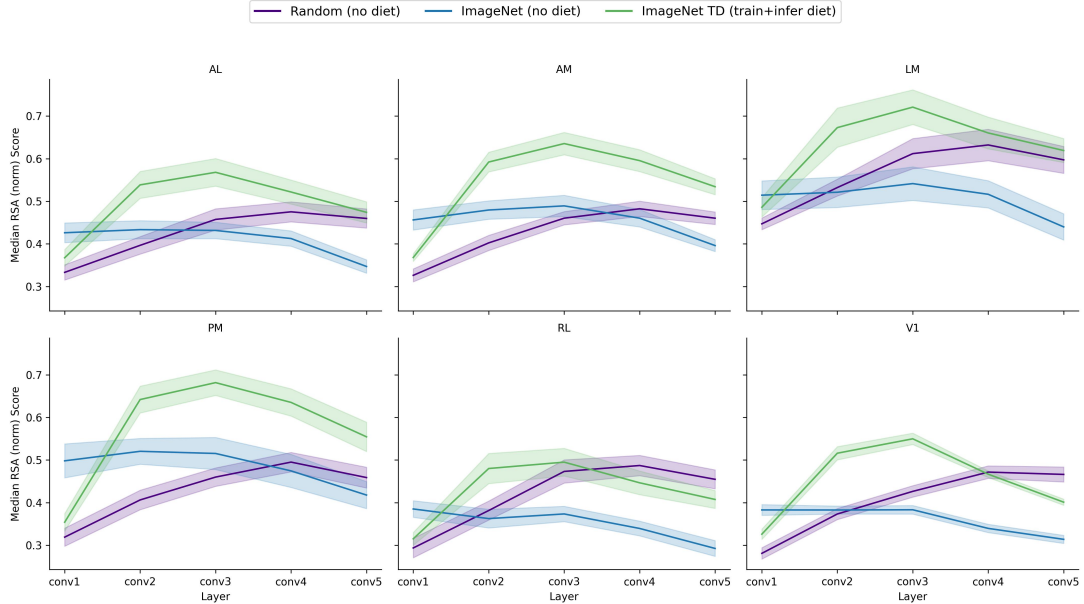


Figure 4: RSA score, normalized to the noise ceiling (pooled interanimal consistency), for all visual areas and for all AlexNet convolutional layers. In **violet** the untrained model, in **blue** the model trained without data diet (inference without diet), in **green** the one trained with data diet (inference with diet).

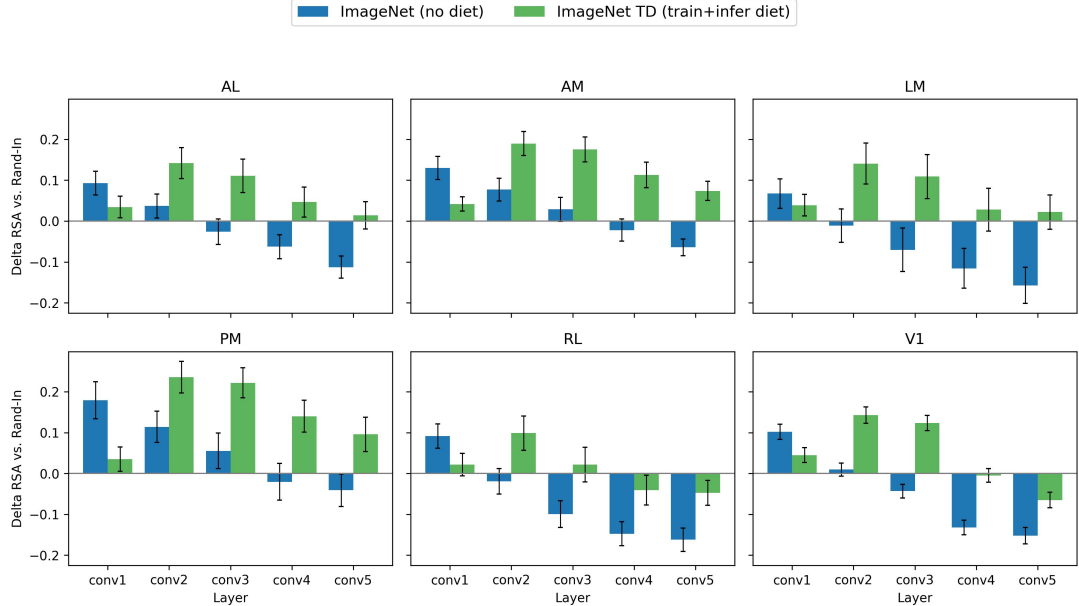


Figure 5: Delta RSA vs untrained model. In **blue** the model trained without data diet (inference without diet), in **green** the one trained with data diet (inference with diet).

3.2 Inference time impact of the diet

Inference time diet Decoupling the diet at train and inference time we can observe that we have similar results also for the model trained on ImageNet dataset without the diet but with data diet at inference time (on Allen stimuli). In fig. 6 we can observe a clear trend in which, except for the first layer, the inference time affects positively the neural predictivity on both the trained model. Specifically we can observe an higher impact on the model trained on ImageNet without data diet: the diet at inference leads to a score similar to the model trained with preprocessed ImageNet.

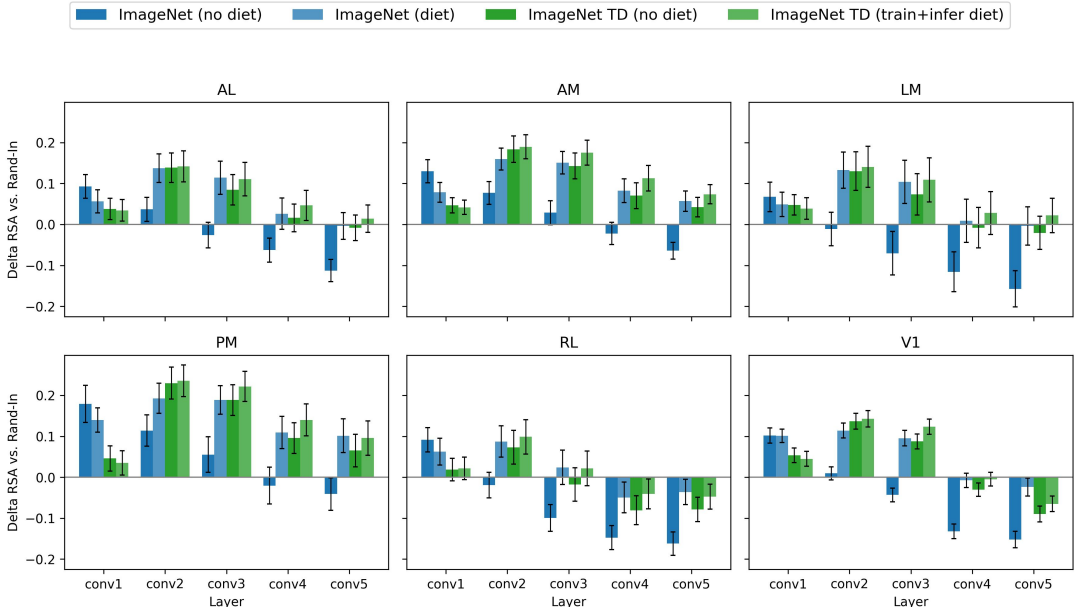


Figure 6: Delta RSA vs untrained model. In **blue** the model trained without data diet (inference without diet), in **light blue** the model trained without data diet but with diet at inference, in **green** the one trained with data diet (inference with diet).

Nayebi diet impact Since we observed that the main effect of the diet is at inference time we decided to explore another data diet, analogous to the one selected by Nayebi [4] as the optimal one. It has been defined as a rescaling of the stimuli to 64×64 followed with an upscaling to 224×224 (in order to match AlexNet input layer).

As we can see from fig. 7, the Nayebi’s diet leads to high RSA score, analogously to our data diet. This means that the up-down scaling procedure may acts like a proxy for the mice vision system. Remarkably this diet provide the best predictivity for the first convolutional layer, hence that conv1 benefits from this procedure.

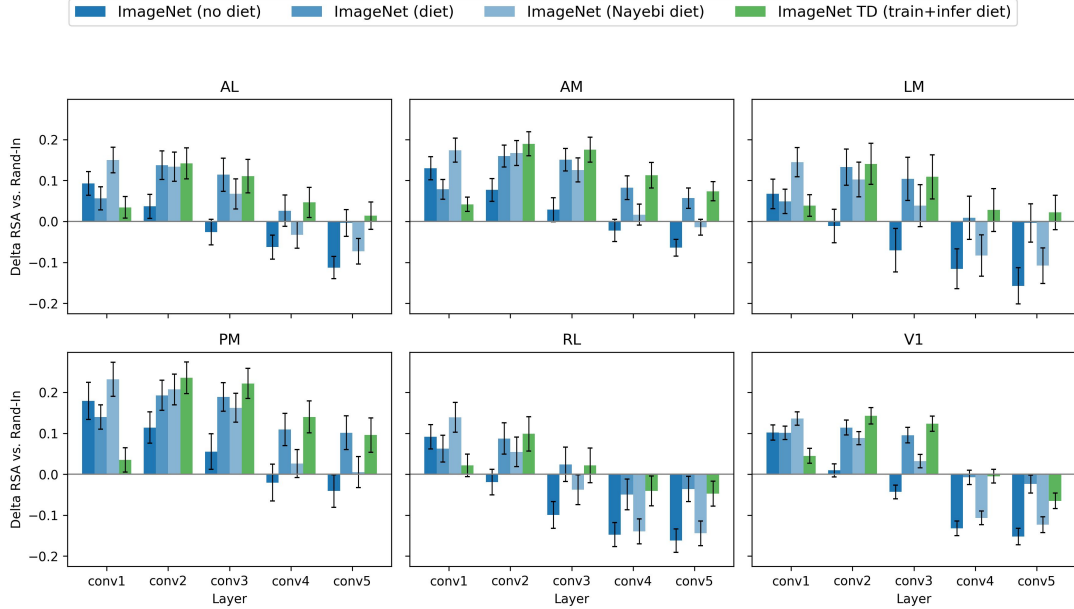


Figure 7: Delta RSA vs untrained model. In **blue** the model trained without data diet (inference without diet), in **light blue** the model trained without data diet but with diet at inference, in **lighter blue** the model trained without data diet but with Nayebi’s diet at inference, in **green** the one trained with data diet (inference with diet).

Random diet impact From fig. 8 we can observe an interesting behaviour: the untrained model with no diet (at inference time) is the one that leads to the highest RSA score in all areas and layers, whereas all the other diets affects negatively the score. This is in contrast with what as been observed on the trained models, that benefits from the diet.

Note that the random diet has been defined with one random value for gaussian blur and gaussian noise therefore is not a robust measure but only a preliminary result. It requires further investigations.

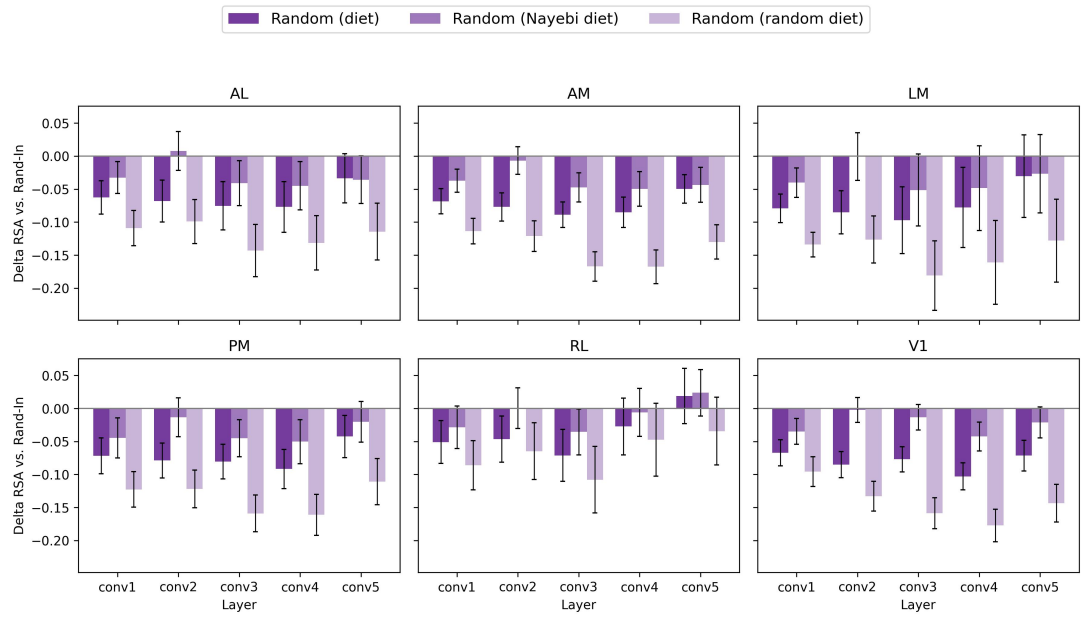


Figure 8: Delta RSA vs untrained model. In lighter shades of violet are shown different data diets (at inference time): our diet, Nayebi's diet and one random diet.

4 Discussion

In this project, we developed a biologically-informed preprocessing pipeline to feed visual stimuli to artificial neural networks that more closely resemble those perceived by mice. We trained AlexNet on the transformed ImageNet dataset and evaluated its neural similarity to biological responses recorded in the Allen Neuropixels dataset.

Our results demonstrate that the ecological data diet, *i.e.*, the one obtained by our preprocessing strategy, provided both at training and inference time, provides the largest neural predictivity for all visual areas and for all convolutional layers of AlexNet, except for the first one (see fig. 5). We note also that in all visual areas the peaks in neural predictivity are always in layers conv2, conv3. Therefore, we do not have evidence of a hierarchical structure in the mouse visual cortex, as already stated by Nayebi *et al.*

We also observed a clear decoupling effect, in the neural predictivity score, if the diet is provided at training or at inference time (see fig. 6). While all tested data diets improved the predictivity of pretrained models, they consistently decreased the predictivity of untrained networks with random weights (see fig. 8). This indicates that the diet engages meaningfully with learned feature representations. In the case of trained models (both with diet and without) the inference time diet always improves the score, but with a clear larger impact on the model trained on unprocessed images, leading to a score almost always close to the one obtained by the model trained on preprocessed images (see fig. 6).

Finally, our attempt to replicate the pseudo-diet proposed by Nayebi—applied in our analysis only at inference time—indicates that the rescaling procedure serves as a reasonable, though not fully optimal, proxy for an ecological diet. Notably, this pseudo-diet yields the highest predictivity scores in the first convolutional layer. This outcome may arise from the construction of the pseudo-diet itself: the rescaling is performed via interpolation, which preserves spatial information, whereas the ecological diet employs a random resize-crop operation that can remove or distort spatial structure. Because the predictivity metric is based on Pearson correlation, any loss of spatial information can eliminate sources of explainable variance. This likely contributes to the decreased performance observed in conv1, a layer whose responses are strongly dependent on the precise spatial arrangement of the input by design.

Our overarching goal was to identify a model of the mouse visual system that incorporates the animal’s natural visual experience. For this reason, we considered the model trained and evaluated with the ecological diet as our reference point, as it consistently processes mouse-like images. Surprisingly, however, most of the improvement in neural alignment originates at inference time: even a network trained on standard high-acuity images shows substantially increased predictivity once mouse-like transformations are applied to its inputs. This suggests that inference-time preprocessing may be the primary driver of alignment with biological neural activity. Consequently, an intriguing possibility emerges: perhaps modifying only the “artificial retina”—the transformations applied at inference—could be sufficient to repurpose a generic vision model such as AlexNet into a plausible “virtual brain” for different species.

Together these findings highlight the importance of stimulus realism in brain-model correspondence analysis. They also reveal that even simple manipulations of input distributions can substantially alter these measurements. Further analyses should explore these directions to better understand how ecological preprocessing shapes the neural alignment of artificial and biological systems.

References

- [1] Allen Institute for Brain Science. *Neuropixels Visual Coding — White Paper v1.0*. White Paper. Accessed: 2025-11-07. Allen Institute for Brain Science, 2024. URL: https://brainmapportal-live-4cc80a57cd6e400d854-f7fdcae.divio-media.net/filer_public/80/75/8075a100-ca64-429a-b39a-569121b612b2/neuropixels_visual_coding_-_white_paper_v10.pdf.
- [2] Nikolaus Kriegeskorte, Marieke Mur, and Peter A. Bandettini. “Representational similarity analysis - connecting the branches of systems neuroscience”. In: *Frontiers in Systems Neuroscience* Volume 2 - 2008 (2008). ISSN: 1662-5137. DOI: [10.3389/neuro.06.004.2008](https://doi.org/10.3389/neuro.06.004.2008). URL: <https://www.frontiersin.org/journals/systems-neuroscience/articles/10.3389/neuro.06.004.2008>.
- [3] Paolo Muratore, Alireza Alemi, and Davide Zoccolan. “Unraveling the complexity of rat object vision requires a full convolutional network and beyond”. In: *Patterns* 6.2 (2025), p. 101149. ISSN: 2666-3899. DOI: <https://doi.org/10.1016/j.patter.2024.101149>. URL: <https://www.sciencedirect.com/science/article/pii/S2666389924003210>.
- [4] Aran Nayebi et al. “Mouse visual cortex as a limited resource system that self-learns an ecologically-general representation”. In: *PLOS Computational Biology* 19.10 (Oct. 2023), pp. 1–36. DOI: [10.1371/journal.pcbi.1011506](https://doi.org/10.1371/journal.pcbi.1011506). URL: <https://doi.org/10.1371/journal.pcbi.1011506>.
- [5] G.T. Prusky and R.M. Douglas. “Characterization of mouse cortical spatial vision”. In: *Vision Research* 44.28 (2004). The Mouse Visual System: From Photoreceptors to Cortex, pp. 3411–3418. ISSN: 0042-6989. DOI: <https://doi.org/10.1016/j.visres.2004.09.001>. URL: <https://www.sciencedirect.com/science/article/pii/S0042698904004390>.